NIH Public Access
Author Manuscript
Nature. Author manuscript; available in PMC 2014 July 11.

Published in final edited form as:
Nature. 2013 July 11; 499(7457): . doi:10.1038/nature12229.

An siRNA screen for NFAT activation identifies septins as coordinators of store-operated Ca^{2+} entry

Sonia Sharma[1,2,*], **Ariel Quintana**[1,2,*], **Gregory M Findlay**[2], **Marcel Mettlen**[3], **Beate Baust**[2], **Mohit Jain**[4,5], **Roland Nilsson**[6], **Anjana Rao**[1,2], and **Patrick G Hogan**[1,2]

[1]La Jolla Institute for Allergy and Immunology, La Jolla, California 92037, USA

[2]Program in Cellular and Molecular Medicine, Children's Hospital Boston, Harvard Medical School, Boston, Massachusetts 02115, USA

[3]The Scripps Research Institute, La Jolla, California 92037, USA

[4]Broad Institute, Cambridge, Massachusetts 02142, USA

[5]Division of Cardiovascular Medicine, Brigham and Women's Hospital, Boston, Massachusetts 02115, USA

[6]Karolinska Institute Stockholm 17176, Sweden

Abstract

The STIM1-ORAI1 pathway of store-operated Ca^{2+} entry is an essential component of cellular Ca^{2+} signaling[1]. STIM1 senses depletion of intracellular Ca^{2+} stores in response to physiological stimuli, and relocalises within the endoplasmic reticulum (ER) to plasma membrane (PM)-apposed junctions, where it recruits and gates open plasma membrane ORAI1 Ca^{2+} channels. Here we used a genome-wide RNAi screen to identify filamentous septin proteins as critical regulators of store-operated Ca^{2+} entry. Septin filaments and phosphatidylinositol 4,5-bisphosphate (PIP2) rearrange locally at ER-PM junctions prior to and during formation of STIM1-ORAI1 clusters, facilitating STIM1 targeting to these junctions and promoting the stable recruitment of ORAI1. Septin rearrangement at junctions is required for PIP2 reorganisation and efficient STIM1-ORAI1 communication. Septins are known to demarcate specialized membrane regions such as dendritic spines, the yeast bud, and the primary cilium, and to serve as membrane diffusion barriers and/or signaling hubs in cellular processes including vesicle trafficking, cell polarity, and cytokinesis[2–4]. Our data show that septins also organise the highly localised plasma membrane domains important in STIM1-ORAI1 signaling, and indicate that septins may organise membrane microdomains relevant to other signaling processes.

Correspondence and requests for materials should be addressed to A.R. (arao@liai.org) and P.G.H. (phogan@liai.org). A.R. and P.G.H. are founders of Calcimedica, Inc (La Jolla, CA).
*These authors contributed equally to this work.

Supplementary Information is linked to the online version of the paper at www.nature.com/nature.

Author Contributions

The genome-wide screen was designed, optimized, and performed by S.S. with assistance from B.B.; S.S. validated septins as regulators of NFAT, store-operated Ca^{2+} entry, STIM1-ORAI1 co-localization and ORAI1 cluster formation, with assistance from G.F. for confocal imaging, CellProfiler analyses and qRT-PCR. A.Q. performed single-cell Ca^{2+} imaging, electrophysiology, TIRFM, STIM1-ORAI1 co-localization, line scan analysis, and FCF experiments, with assistance from M.M. for TIRFM. M.J. and R.N. performed bioinformatic analyses. P.G.H. and A.R. provided overall direction and supervised project planning and execution. S.S., A.Q., P.G.H. and A.R. wrote the manuscript with input from other authors.

The remaining authors state that they have no competing interests.

NIH-PA Author Manuscript
NIH-PA Author Manuscript
NIH-PA Author Manuscript

NIH-PA Author Manuscript

NIH-PA Author Manuscript

NIH-PA Author Manuscript

Ca^{2+}-regulated NFAT transcription factors are activated by sustained Ca^{2+} influx across the plasma membrane[5]. We previously used a Ca^{2+}-responsive NFAT1-GFP reporter protein in *Drosophila* RNAi screens that identified ORAI1 as a Ca^{2+} channel responsible for sustained physiological Ca^{2+} influx dependent on store-operated Ca^{2+} entry[6], and DYRK-family kinases as negative regulators of NFAT signaling[7,8]. To identify new modulators of Ca^{2+}/NFAT signalling, we performed a genome-wide RNAi screen in HeLa cells stably expressing NFAT1-GFP (Methods and Supplementary Fig. 1).

Septin 4 was a hit that emerged early in the screen. siRNA-mediated depletion of *SEPT4* decreased Ca^{2+}-induced NFAT nuclear translocation by >95%, an effect similar in magnitude to that observed upon depletion of STIM1 or ORAI1 (Fig. 1a, Supplementary Fig. 2a). Of the original siRNAs in the *siSEPT4* pool, only *#3* and *#4* (Supplementary Table 1) strongly inhibited NFAT activation induced by the SERCA inhibitor thapsigargin (TG) (Supplementary Fig. 2b); these siRNAs also depleted septin 5 and to a lesser extent the abundant septin 2 (Supplementary Fig. 2c–f). When siRNAs individually targeting SEPT2, SEPT4 and SEPT5 were tested, all three were needed to decrease NFAT nuclear translocation (Supplementary Fig. 2g). Reconstitution with siRNA-resistant septin 4, septin 5 or both rescued NFAT nuclear translocation (Fig. 1b, c). In subsequent experiments, we used both *siSEPT4* #3 and *siSEPT4 #4* (hereafter *siSEPT*).

Septins modulate store-operated Ca^{2+} entry, rather than events downstream of Ca^{2+} entry. In plate-reader assays[9], treatment of HeLa cells with *siSEPT* decreased the sustained cytoplasmic Ca^{2+} response to thapsigargin in Ca^{2}-containing medium (Fig. 1d), without affecting Ca^{2+} release from ER stores (Supplementary Fig. 3a). At the single-cell level, *siSEPT*-treated Jurkat and HeLa cells showed a substantial decrease in the cytoplasmic Ca^{2+} signal after store depletion, with minimal effects on Ca^{2+} release from ER stores (Fig. 1e, Supplementary Fig. 3b, c). Septins directly affected Ca^{2+} entry. The activity of the plasma membrane Ca^{2+} ATPase (PMCA) was not affected by septin depletion (Supplementary Fig. 3d), and the observed effects of septin depletion on Ca^{2+} influx were not secondary to changes in membrane potential (Supplementary Fig. 3e). Septin depletion significantly slowed the quenching of intracellular fura-2 fluorescence by influx of extracellular Mn^{2+}, a surrogate for Ca^{2+}, providing strong evidence that septins regulate Ca^{2+} influx channels (Supplementary Fig. 3f). Finally, whole cell patch-clamp recording demonstrated a significant reduction in store-operated Ca^{2+} current (I_{crac}) in *siSEPT*-treated cells (Fig. 1f). Thus septin depletion acts upstream of Ca^{2+} entry to reduce Ca^{2+} influx through CRAC/ORAI1 channels.

ORAI1 channels are functional in septin-depleted cells. Soluble fragments of the STIM1 C-terminus (STIM1-CT) gate ORAI1 channels *in vitro*[10] and produce constitutive Ca^{2+} influx in cells[11–14]. Expression of mCherry-STIM1-CT(233–473) in HeLa-NFAT1-GFP cells induced nuclear accumulation of NFAT in the absence of stimulation (Fig. 1g, *1st and 3rd clusters, compare red bars*). Treatment with *siSEPT* prevented nuclear import of NFAT in response to thapsigargin as expected (Fig. 1g, *1st and 2nd clusters, compare black bars*), but mCherry-STIM1-CT(233–473) induced constitutive NFAT nuclear localisation to the same extent as in the *siControl*-treated cells (Fig. 1g, *3rd and 4th clusters, compare red bars*). NFAT activation was dependent on Ca^{2+} influx and Ca^{2+}-calcineurin signaling, since it was abolished by the calcineurin inhibitor cyclosporin A (CsA; Fig. 1g, *pink bars*). Thus, in septin-depleted cells, physiological STIM1-mediated activation of ORAI1 is impaired but the ORAI1 channel itself is intact and can be gated by soluble STIM1.

These findings implied that the defect might lie in inefficient relocalisation of STIM1 or ORAI1 to ER-plasma membrane junctions following ER Ca^{2+} store depletion. Indeed, *siSEPT*-treated HeLa cells stably expressing low levels of GFP-STIM1 and mCherry-

NIH-PA Author Manuscript

NIH-PA Author Manuscript

NIH-PA Author Manuscript

ORAI1 showed significantly decreased STIM1-ORAI1 colocalisation at ER-plasma membrane junctions after thapsigargin treatment, compared to *siControl*-treated cells (Fig. 2a). The areas and intensities of STIM1 puncta were not altered significantly (Supplementary Fig. 4). In cells expressing only endogenous ORAI1, *siSEPT* treatment resulted in a decrease in both the rate and extent of GFP-STIM1 translocation to the vicinity of the plasma membrane after thapsigargin stimulation, as measured by live-cell total internal reflection fluorescence microscopy (TIRFM) (Fig. 2b, *compare blue and black traces*). When both endogenous ORAI1 and septins were depleted, GFP-STIM1 accumulation was even further impaired (Fig. 2b, *green trace*). Since reduced accumulation of STIM1 could arise from a defect in maintenance of ER-plasma membrane junctions, we rendered junctional and near-junctional ER visible to TIRFM using a fluorescent ER-targeted marker (Supplementary Fig. 5a). Septin-depleted cells did not show a significant change in ER fluorescence at the TIRF layer (Supplementary Fig. 5b), indicating that the junctions are present and grossly normal at the light microscope level. These experiments show that septins facilitate STIM1 recruitment to ER-plasma membrane junctions.

TIRFM revealed aberrant ORAI1 distribution and cluster formation in the plasma membrane of septin-depleted cells. In resting cells, the histogram of mCherry-ORAI1 pixel intensities for *siSEPT*-treated cells had a prominent shoulder extending to higher intensities, in contrast to the symmetrical distribution seen in *siControl*-treated cells (Fig. 2c). Correspondingly, surface plots of mCherry-ORAI1 pixel intensities showed prominent, jagged peaks in *siSEPT*-treated cells, compared to the more even ORAI1 distribution in *siControl*-treated cells (Fig. 2c, *surface plots, bottom left*). After thapsigargin stimulation, septin-depleted cells showed fewer distinct mCherry-ORAI1 peaks than control cells by visual inspection (Fig. 2c, *surface plots, bottom right*), and quantification revealed a significant reduction in the number of ORAI1 clusters (Fig. 2d). The amount of STIM1-GFP at the plasma membrane was similar in *siControl* and *siSEPT*-treated HeLa cells expressing mCherry-ORAI1 (Supplementary Fig. 5c), and the total levels of mCherry-ORAI1, assessed by western blotting and flow cytometry, were unchanged upon septin depletion (data not shown). Thus ORAI1 is disorganised prior to store depletion, and ORAI1 clusters form poorly after store depletion and are unstable in *siSEPT*-treated cells.

We examined the cellular localisation of septins relative to GFP-STIM1 and mCherry-ORAI1 by confocal and TIRF microscopy of *siSEPT*-treated HeLa cells reconstituted with low levels of siRNA-resistant, BFP-tagged septin 4. Septin 4 and ORAI1 were both broadly distributed in the plasma membrane in resting cells (Fig. 3a); after 10 min of thapsigargin stimulation, STIM1 and ORAI1 co-localised as expected, whereas septin 4 formed distinct clusters that did not colocalise with ORAI1 or STIM1 at ER-PM junctions (Fig. 3b, c; Supplementary Fig. 6a). Rather, STIM1 translocation to junctional ER after Ca^{2+} store depletion was accompanied by a biphasic reorganisation of septin at the plasma membrane (Fig. 3d, e, Supplementary Fig. 6b, c). Septin 4 fluorescence in the TIRF plane initially increased modestly at approximately the same time that STIM1-ORAI1 clusters began to form (Fig. 3d, e and Supplementary Fig. 6c, *top panel*). Following the initial increase, septin 4 fluorescence at the TIRF layer decreased, with the magnitude of the decrease dependent on Ca^{2+} influx (Supplementary Fig. 6c, *compare top and bottom panels*). ORAI1 clusters began to form only as the level of septin 4 at the TIRF layer decreased (Fig. 3e, Supplementary Fig. 6b). The septin 4 that remained at the TIRF layer coalesced into distinct small clusters that did not colocalise with ORAI1 clusters (Fig. 3c, Supplementary Fig. 6d), supporting the conclusion that septin 4 is not enriched at ER-plasma membrane junctions where mature STIM1-ORAI1 complexes form.

To test whether septin rearrangement is required for redistribution of ORAI1 after ER Ca^{2+} store depletion, we used forchlorfenuron (FCF), a small molecule that perturbs the normal

NIH-PA Author Manuscript

NIH-PA Author Manuscript

NIH-PA Author Manuscript

dynamics of septins in yeast and mammalian cells by hyperpolymerising and stabilising septin filaments[15,16]. Preincubating HeLa cells with 100–200 μM FCF sharply reduced store-operated Ca^{2+} influx without affecting ER Ca^{2+} stores, and the combination of FCF and septin RNAi had a stronger effect (Fig. 4a). Neither STIM1 translocation to ER-plasma membrane junctions (Fig. 4b) nor constitutive ORAI activation by STIM1-CT(233–473) (Fig. 4c) was impaired in FCF-treated cells. However, FCF treatment abolished the formation of mCherry-ORAI1 clusters (Fig. 4d) and diminished STIM1-ORAI1 colocalisation at the TIRF layer in response to thapsigargin stimulation (Fig. 4e, Supplementary Fig. 7). Thus, immobilisation of septin filaments with FCF inhibits ORAI1 cluster formation, STIM1-ORAI1 colocalisation, and store-operated Ca^{2+} influx.

Phosphoinositides are implicated in STIM-ORAI signaling: the polybasic region at the STIM1 C-terminus targets STIM1 to the plasma membrane[17,18] through interactions with PIP2 and PIP3[19–21]. Septins also bind phosphoinositides, in part through a conserved polybasic region[22,23] which in mammalian SEPT4 preferentially binds PIP2 and to a lesser extent PIP3[22]. We therefore asked whether septin reorganisation during STIM-ORAI signalling correlated with changes in the distribution of plasma membrane phosphoinositides. We used the pleckstrin homology (PH) domain of PLCδ, which binds the PIP2 headgroup with high specificity[24,25], as a probe for accessible PIP2 in the plasma membrane. BFP-septin 4, BFP-septin 5, and PIP2 accumulated preferentially in the circumference of the mCherry-ORAI1 clusters that form in control cells after thapsigargin or histamine stimulation, either in the absence or presence of extracellular Ca^{2+}; in contrast, there was no reorganisation of PIP2 around ORAI1 clusters in septin-depleted cells (*line scans* in Fig. 5a and Supplementary Fig. 8a, b). In control cells expressing tagged ORAI1 and PH-PLCδ and treated with thapsigargin or histamine, PIP2 was cleared from the membrane at sites of ORAI1 cluster formation (Fig. 5b, Supplementary Fig. 8c); in septin-depleted cells, it remained uniformly distributed after ER Ca^{2+} store depletion (Fig. 5b). This difference in the local PIP2 environment is evident in the ratio of the GFP-PLCδ-PH signal within ORAI1 clusters to the signal in the immediate surrounding membrane (Supplementary Fig. 8d).

In *siControl*-treated cells, the coefficient of variation (CV) of the PIP2 TIRFM signal across the cell increased after thapsigargin treatment (Supplementary Fig. 9a), indicating that PIP2, which is distributed relatively uniformly in resting cells (data not shown), is less uniformly distributed after stimulation (also see Fig 5b, Supplementary Fig. 8c). This increase in CV was barely observed in septin-depleted cells (Supplementary Fig. 9a), a result that cannot be explained by a failure to respond to thapsigargin, since *siControl* and *siSEPT*-treated cells showed similar reductions in the global plasma membrane GFP-PLCδ-PH signal after thapsigargin treatment (Supplementary Fig. 9b). Together these results indicate that localised microdomains of PIP2 arise in the plasma membrane after stimulation, and that septins shape these PIP2 membrane domains in the vicinity of the CRAC channel.

Our findings demonstrate for the first time that septins play a key role in store-operated Ca^{2+} entry (Supplementary Fig. 10, Supplementary Discussion). Septins are required for proper organisation of ORAI1 in the plasma membrane even before depletion of ER Ca^{2+} stores. They promote the later stages of the approach of STIM1 to ER-plasma membrane junctions and the formation of stable ORAI1 clusters after store depletion. Upon stimulation, septins redistribute at the plasma membrane, and their redistribution correlates temporally with both STIM1 translocation and formation of ORAI1 clusters. Finally, septins define a lipid microdomain around the STIM-ORAI complex that correlates with STIM-ORAI complex stability. Our data set the stage for further investigations of how septin reorganisation might choreograph the physiological interactions between STIM1 and ORAI1 in store-operated Ca^{2+} entry, and raise the possibility that septins define not just the cellular regions involved

NIH-PA Author Manuscript

NIH-PA Author Manuscript

NIH-PA Author Manuscript

in a few specialized signalling processes[26–28] but also plasma membrane microdomains that underlie many other signalling processes.

Methods

Genome-wide siRNA screen

The screen was performed at the Institute for Chemistry and Cell Biology (ICCB) (Boston, MA). HeLa cells stably expressing NFAT1(1–460)-GFP[7,8] and STIM1-mDsRed, and transiently expressing FLAG-ORAI1, were transfected in duplicate with 21,757 siRNA oligonucleotide pools (Human siGenome, 4 siRNA oligonucleotides/pool, Dharmacon) arrayed in 384-well plates, using HiPerfect transfection reagent (QIAGEN) at 20 nM. After 72 h, cells were stimulated with 250 nM thapsigargin for 90 min at room temperature in full growth media, and imaged for NFAT1-GFP and DAPI (nuclear) fluorescence. For each plate, an initial mean score of NFAT1-GFP nuclear translocation was calculated (see below), using data from all experimental wells. Data from outlier wells with translocation scores >3 s.d. from this mean (i.e. likely to be true hits) were discarded, and the mean and s.d. were recalculated. Each well was assigned a Z score for NFAT1-GFP nuclear translocation, representing the number of standard deviations from the recalculated mean. Detailed follow-up studies to verify candidates and exclude off-target effects have not yet been completed. Supplementary Fig. 1 lists all the provisional candidates from the initial screen: genes that potentially encode positive regulators of NFAT1-GFP nuclear translocation, as defined by siRNA pools which (in duplicate wells) decreased NFAT nuclear translocation with an average Z score of ≤ −2.0. siRNAs associated with duplicate or discontinued EntrezGene identifiers have been removed.

Quantification of nuclear translocation

Nuclear translocation of NFAT1-GFP was scored from fluorescent images as previously described[8,29]. Briefly, confluent monolayers in black rim, clear bottom 384-well or 96-well microplates (Corning/Costar) were stimulated in complete growth media supplemented with 250 nM or 1 μM TG and 2 mM $CaCl_2$. Wells were scored for NFAT1-GFP nuclear translocation, defined as the percentage of all cells showing ≥ 70% of NFAT-GFP fluorescence overlapping with DAPI fluorescence. Except for the initial screen, each data point represents the average of 3 separate wells on a plate (>1200 cells per well), with error bars reporting s.d. between wells and experiments represent biological replicates between 3–5 independent experiments. CsA pre-treatments were performed for 30 min at 1 μM.

Ca^{2+} influx assays

Cytoplasmic Ca^{2+} was monitored using fura-2 in live cells stimulated with 1 μM TG. For plate-reader assays, confluent monolayers of NFAT1-GFP, STIM1-mDsRed and FLAG-ORAI1-expressing HeLa cells were seeded in black-rim, clear-bottom 96-well plates (Corning/Costar) the day before analysis. Cells were loaded with 1–2 μM fura-2/AM in modified Ringer's solution (mM): 20 HEPES, 125 NaCl, 5 KCl, 1.5 $MgCl_2$, 1.5 $CaCl_2$, 10 D-glucose (pH 7.4 with NaOH) supplemented with 2.5 mM probenecid (Sigma). After 20 min at room temperature in the dark, cells were washed twice in modified Ringer's solution and probenecid, and incubated for 30 min. Time-lapse fluorescence was recorded at 5 sec intervals on a FlexStation III (Molecular Devices), using dual 340/380 nm excitation, with emission recorded at 510 nm. Data are represented as 340/380 emissions over time. For single-cell Ca^{2+} imaging, HeLa or Jurkat cells were plated on 18 mm coverslips and loaded with 3 μM fura-2/AM for 30–45 min at 37°C in DMEM containing 2.5 mM probenecid and 10 mM HEPES, washed twice with fresh media, and analysed immediately. Coverslips were assembled into a chamber on the stage of an Olympus IX 71 microscope equipped with an Olympus UPLSAPO 20×, N.A 0.75 objective. Cells were alternately illuminated at 340 and

NIH-PA Author Manuscript

NIH-PA Author Manuscript

NIH-PA Author Manuscript

380 nm with the Polychrome V monochromator (TILL Photonics) using ET Fura filter (Chroma Technology Corp, cat. 79001). The fluorescence emission at λ > 400 nm (LP 400 nm, Emitter 510/80 nm) were captured with a CCD camera (SensiCam, TILL Imago), digitized and analyzed by TILL Vision software. Ratio images were recorded at intervals of 2 sec. Ca^{2+}concentration was estimated from the relation $[Ca^{2+}]_i = K*(R-R_{min})/(R_{max}-R)$, where the values of K, R_{min}, and R_{max} were determined from an in situ calibration of fura-2 in HeLa cells as described[30]. Ca^{2+} Ringer's solution contained 1 mM $CaCl_2$ (for Jurkat T cells) or 2 mM $CaCl_2$ (for HeLa cells). 1 mM EGTA was substituted for $CaCl_2$ in the 0-Ca^{2+} Ringer's solution. High-K^+ Ringer's solution contained 145 mM K^+, 10 mM Na^+, and 5 mM Ca^{2+}. Data were analyzed using TILL Vision (TILL Photonics) and Igor Pro (WaveMetrics). 3–5 experiments were performed for each condition and error bars report mean ± s.e.m. Statistical significance was determined using an unpaired, two-sided Student's t-test.

Electrophysiology

Patch-clamp experiments were performed in the whole cell configuration at 21–25 °C. Micro-pipettes with a resistance of 2.5–3.2 MΩ were pulled and fire-polished. To reduce electrode capacitance, pipettes were dipped into Sigma-coat immediately before use. Membrane currents were acquired with an EPC-9 patch-clamp amplifier (HEKA). Voltage ramps of 200 ms duration spanning a range of −150 to + 100 mV were delivered from a holding potential of 0 mV at a rate of 0.5 Hz over a period of 400 s. All voltages were corrected for a liquid junction potential of −10 mV between internal and bath solutions. Currents were filtered at 2.9 kHz and digitized at a sampling rate of 10 kHz. Pipette and cell capacitance were electronically cancelled before each voltage ramp. Background current measured in the first voltage ramp after break-in was subtracted. For display, currents were digitally filtered offline at 1 kHz. Current amplitudes at −130 mV from individual voltage ramp current were used to depict the temporal development of currents. Averaged data are given as mean ± s.e.m. for *n* cells. External solution was (in mM): 120 NaCl, 2 $MgCl_2$, 10 $CaCl_2$, 10 TEA-Cl, 10 HEPES, 10 glucose, pH 7.2 with NaOH. Pipette solution contained (in mM): 0.05 $InsP_3$, 5×10^{-5} TG, 140 Cs-glutamate, 12 EGTA, 3 $MgCl_2$, 10 HEPES, pH 7.2 with CsOH.

TIRF microscopy

TIRF was performed using Nikon CFI Apo objectives (100×, 1.49 NAl; or 60×, 1.45 NA) mounted on a Ti-Eclipse inverted microscope with Perfect Focus System (PFS; Nikon). Imaging was performed on HeLa cells expressing GFP-STIM1, mCherry-ORAI1, BFP-septin or other probes as indicated. Time-lapse sequences from 4–7 (100×) or 7–12 (60×) cells were acquired by sequential, nearly simultaneous acquisition of individual images using a Coolsnap HQ2 monochrome CCD camera (Photometrics, Tuscon, AZ). Exposure times were 100 msec and 180 msec (for 488 nm and 561 nm channels, respectively) at a frame-rate of 20 sec. For co-localization, ImageJ macro JACoP was used. Data were analyzed using ImageJ (NIH), Igor Pro (WaveMetrics) and Excel (Microsoft). 3–5 experiments were performed for each condition and error bars report mean ± s.e.m. In case data points were normally distributed, an unpaired, two-sided Student's t-test was used. If a normal distribution could not be confirmed, a non-parametric test (Mann-Whitney) was carried out.

Supplementary Material

Refer to Web version on PubMed Central for supplementary material.

NIH-PA Author Manuscript

NIH-PA Author Manuscript

NIH-PA Author Manuscript

Acknowledgments

We thank C. Shamu, S. Rudnicki, S. Johnston, and D. Wrobel at ICCB for screening support; A. Carpenter and M. Bray for CellProfiler optimization; P. Meraner and Y. Zhou for cell lines and constructs; S. Schmid (The Scripps Research Institute) and James Fitzpatrick (Waitt Advanced Biophotonics Center at the Salk Institute) for TIRF microscope access; C. Junker at Saarland University for the RFP-ER construct; Seth Field at UCSD for the GFP-PLCδ-PH plasmid; S. Schmid for manuscript review. The work was supported by NIH R01 grants AI40127 and AI84167 (to A.R. and P.G.H.), NIH RC4 grant AI092763 (to A.R. and S.S.); a Fellowship from the Canadian Institutes for Health Research and a Special Fellowship from the Leukemia and Lymphoma Society (to S.S.); postdoctoral fellowship QU298/1–1 from the Deutsche Forschungsgemeinschaft (to A.Q.); NIH grant K08 HL107451 (to M.J.); a postdoctoral scholarship from the Knut & Alice Wallenberg Foundation (to R.N.); NIH R01 grant R01GM73165 (to S. Schmid, which supports M.M.).

References

1. Hogan PG, Lewis RS, Rao A. Molecular basis of calcium signaling in lymphocytes: STIM and ORAI. Annu Rev Immunol. 2010; 28:491–533.10.1146/annurev.immunol.021908.132550 [PubMed: 20307213]
2. Estey MP, Kim MS, Trimble WS. Septins. Curr Biol. 2011; 21:R384–387.10.1016/j.cub.2011.03.067 [PubMed: 21601794]
3. Caudron F, Barral Y. Septins and the lateral compartmentalization of eukaryotic membranes. Dev Cell. 2009; 16:493–506.10.1016/j.devcel.2009.04.003 [PubMed: 19386259]
4. Mostowy S, Cossart P. Septins: the fourth component of the cytoskeleton. Nat Rev Mol Cell Biol. 2012; 13:183–194.10.1038/nrm3284 [PubMed: 22314400]
5. Hogan PG, Chen L, Nardone J, Rao A. Transcriptional regulation by calcium, calcineurin, and NFAT. Genes Dev. 2003; 17:2205–2232.10.1101/gad.1102703 [PubMed: 12975316]
6. Feske S, et al. A mutation in Orai1 causes immune deficiency by abrogating CRAC channel function. Nature. 2006; 441:179–185.10.1038/nature04702 [PubMed: 16582901]
7. Gwack Y, et al. A genome-wide Drosophila RNAi screen identifies DYRK-family kinases as regulators of NFAT. Nature. 2006; 441:646–650.10.1038/nature04631 [PubMed: 16511445]
8. Sharma S, et al. Dephosphorylation of the nuclear factor of activated T cells (NFAT) transcription factor is regulated by an RNA-protein scaffold complex. Proc Natl Acad Sci U S A. 2011; 108:11381–11386.10.1073/pnas.1019711108 [PubMed: 21709260]
9. Liou J, et al. STIM is a Ca^{2+} sensor essential for Ca^{2+}-store-depletion-triggered Ca^{2+} influx. Curr Biol. 2005; 15:1235–1241.10.1016/j.cub.2005.05.055 [PubMed: 16005298]
10. Zhou Y, et al. STIM1 gates the store-operated calcium channel ORAI1 in vitro. Nat Struct Mol Biol. 2010; 17:112–116.10.1038/nsmb.1724 [PubMed: 20037597]
11. Huang GN, et al. STIM1 carboxyl-terminus activates native SOC, I_{crac} and TRPC1 channels. Nat Cell Biol. 2006; 8:1003–1010.10.1038/ncb1454 [PubMed: 16906149]
12. Muik M, et al. A cytosolic homomerization and a modulatory domain within STIM1 C terminus determine coupling to ORAI1 channels. J Biol Chem. 2009; 284:8421–8426.10.1074/jbc.C800229200 [PubMed: 19189966]
13. Muik M, et al. Dynamic coupling of the putative coiled-coil domain of ORAI1 with STIM1 mediates ORAI1 channel activation. J Biol Chem. 2008; 283:8014–8022.10.1074/jbc.M708898200 [PubMed: 18187424]
14. Zhang SL, et al. Store-dependent and -independent modes regulating Ca^{2+} release-activated Ca^{2+} channel activity of human Orai1 and Orai3. J Biol Chem. 2008; 283:17662–17671.10.1074/jbc.M801536200 [PubMed: 18420579]
15. Hu Q, Nelson WJ, Spiliotis ET. Forchlorfenuron alters mammalian septin assembly, organization, and dynamics. J Biol Chem. 2008; 283:29563–29571.10.1074/jbc.M804962200 [PubMed: 18713753]
16. DeMay BS, Meseroll RA, Occhipinti P, Gladfelter AS. Cellular requirements for the small molecule forchlorfenuron to stabilize the septin cytoskeleton. Cytoskeleton (Hoboken). 2010; 67:383–399.10.1002/cm.20452 [PubMed: 20517926]

NIH-PA Author Manuscript

NIH-PA Author Manuscript

NIH-PA Author Manuscript

17. Li Z, et al. Mapping the interacting domains of STIM1 and Orai1 in Ca^{2+} release-activated Ca^{2+} channel activation. J Biol Chem. 2007; 282:29448–29456.10.1074/jbc.M703573200 [PubMed: 17702753]
18. Park CY, et al. STIM1 clusters and activates CRAC channels via direct binding of a cytosolic domain to Orai1. Cell. 2009; 136:876–890.10.1016/j.cell.2009.02.014 [PubMed: 19249086]
19. Walsh CM, et al. Role of phosphoinositides in STIM1 dynamics and store-operated calcium entry. Biochem J. 2010; 425:159–168.10.1042/BJ20090884 [PubMed: 19843011]
20. Ercan E, et al. A conserved, lipid-mediated sorting mechanism of yeast Ist2 and mammalian STIM proteins to the peripheral ER. Traffic. 2010; 10:1802–1818.10.1111/j.1600-0854.2009.00995x [PubMed: 19845919]
21. Liou J, Fivaz M, Inoue T, Meyer T. Live-cell imaging reveals sequential oligomerization and local plasma membrane targeting of stromal interaction molecule 1 after Ca^{2+} store depletion. Proc Natl Acad Sci U S A. 2007; 104:9301–9306.10.1073/pnas.0702866104 [PubMed: 17517596]
22. Zhang J, et al. Phosphatidylinositol polyphosphate binding to the mammalian septin H5 is modulated by GTP. Current Biology. 1999; 9:1458–1467. [PubMed: 10607590]
23. Bertin A, et al. Phosphatidylinositol-4,5-bisphosphate promotes budding yeast septin filament assembly and organization. J Mol Biol. 2010; 404:711–731.10.1016/j.jmb.2010.10.002 [PubMed: 20951708]
24. Varnai P, Balla T. Visualization of phosphoinositides that bind pleckstrin homology domains: calcium- and agonist-induced dynamic changes and relationship to myo-[^{3}H]inositol-labeled phosphoinositide pools. J Cell Biol. 1998; 143:501–510. [PubMed: 9786958]
25. Stauffer TP, Ahn S, Meyer T. Receptor-induced transient reduction in plasma membrane PtdIns(4,5)P_2 concentration monitored in living cells. Curr Biol. 1998; 8:343–346. [PubMed: 9512420]
26. Yang YM, et al. Septins regulate developmental switching from microdomain to nanodomain coupling of Ca^{2+} influx to neurotransmitter release at a central synapse. Neuron. 2010; 67:100–115.10.1016/j.neuron.2010.06.003 [PubMed: 20624595]
27. Hu Q, et al. A septin diffusion barrier at the base of the primary cilium maintains ciliary membrane protein distribution. Science. 2010; 329:1–5.
28. Tada T, et al. Role of septin cytoskeleton in spine morphogenesis and dendrite development in neurons. Curr Biol. 2007; 17:1752–1758.10.1016/j.cub.2007.09.039 [PubMed: 17935993]
29. Oh-Hora M, et al. Dual functions for the endoplasmic reticulum calcium sensors STIM1 and STIM2 in T cell activation and tolerance. Nat Immunol. 2008; 9:432–443.10.1038/ni1574 [PubMed: 18327260]
30. Grynkiewicz G, Poenie M, Tsien RY. A new generation of Ca^{2+} indicators with greatly improved fluorescence properties. J Biol Chem. 1985; 260:3440–3450. [PubMed: 3838314]

NIH-PA Author Manuscript
NIH-PA Author Manuscript
NIH-PA Author Manuscript

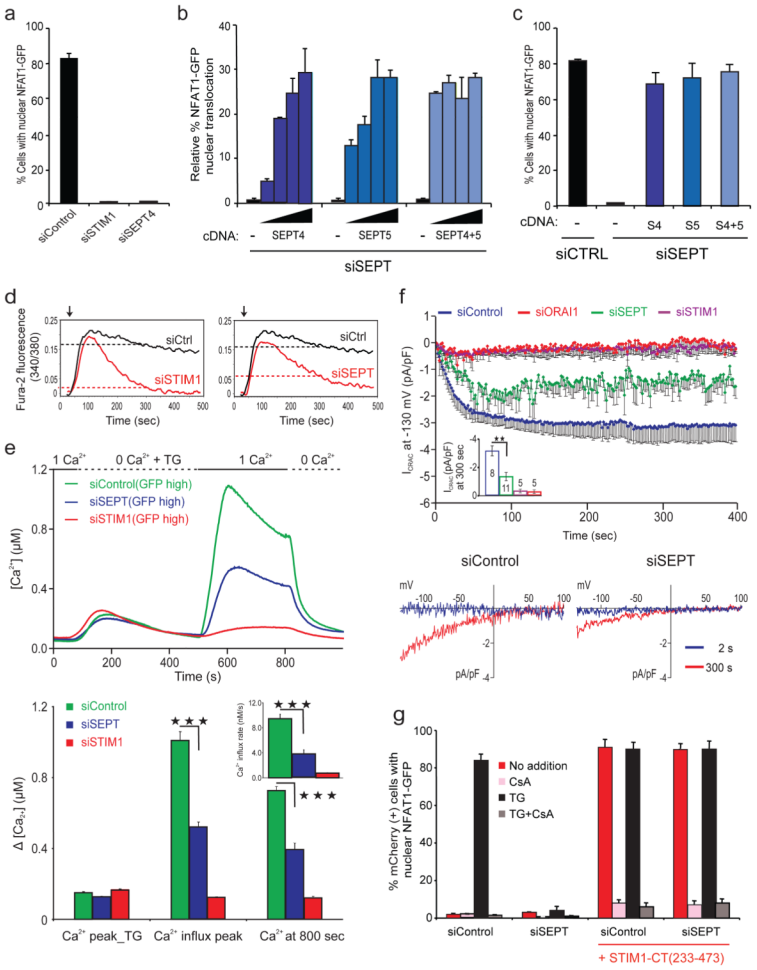

Figure 1. Mammalian septin proteins are essential regulators of NFAT activation and store-operated Ca^{2+} influx

a, HeLa NFAT1-GFP cells were transfected with siRNAs, stimulated with thapsigargin (TG) and scored for nuclear NFAT1 by fluorescence imaging and automated analysis. **b**, siRNA-treated HeLa NFAT1-GFP cells were transfected with siRNA-resistant *SEPT4* and *SEPT5* cDNAs (5, 10, 15, 20 ng), stimulated with TG and scored for nuclear NFAT1. The (−) cDNA samples received empty vector (20 ng). **c**, Reanalysis of **b** (20 ng) after gating on septin-expressing cells. **d**, Averaged $[Ca^{2+}]_i$ readings in siRNA-treated, fura-2 loaded HeLa NFAT1-GFP cells stimulated with TG (*arrow*) in 10 mM $[Ca^{2+}]_o$. The same siControl trace is shown in both panels. **e**, (*Upper*) Single-cell $[Ca^{2+}]_i$ measurements in siRNA-treated, fura-2 loaded Jurkat T cells expressing high levels of co-transfected GFP (*siControl, n=135; siSTIM1, n=212; siSEPT, n=120)* exposed to 0 or 1 mM $[Ca^{2+}]_o$ before and after TG stimulation. (*Lower*) $[Ca^{2+}]_I$ at the peak of TG-stimulated release from ER stores in GFP-high cells; at the peak following Ca^{2+} add-back (*siSEPT vs siControl, $p=5.3\times10^{-22}$)*; and at 800 sec (*siSEPT vs siControl, $p=1.6\times10^{-16}$); inset*, initial rates of $[Ca^{2+}]_i$ increase (*siSEPT vs siControl, $p=1.4\times10^{-13}$)*. Triple asterisks indicate statistically significant differences. **f**, (*Upper*) CRAC current density at −130 mV in Jurkat T cells; *inset*, CRAC current density at 300 sec (*siSEPT vs siControl, p=0.002*). (*Lower*) Current–voltage relationship recorded 2 sec and 300 sec after break-in (whole cell configuration) **g**, mCherry or mCherry-STIM1-CT(233–473) plasmids were expressed in siRNA-treated HeLa NFAT1-GFP cells, and

mCherry-positive cells were stimulated and scored for nuclear NFAT1. Error bars report sample standard deviation (s.d.).

NIH-PA Author Manuscript
NIH-PA Author Manuscript
NIH-PA Author Manuscript

NIH-PA Author Manuscript
NIH-PA Author Manuscript
NIH-PA Author Manuscript

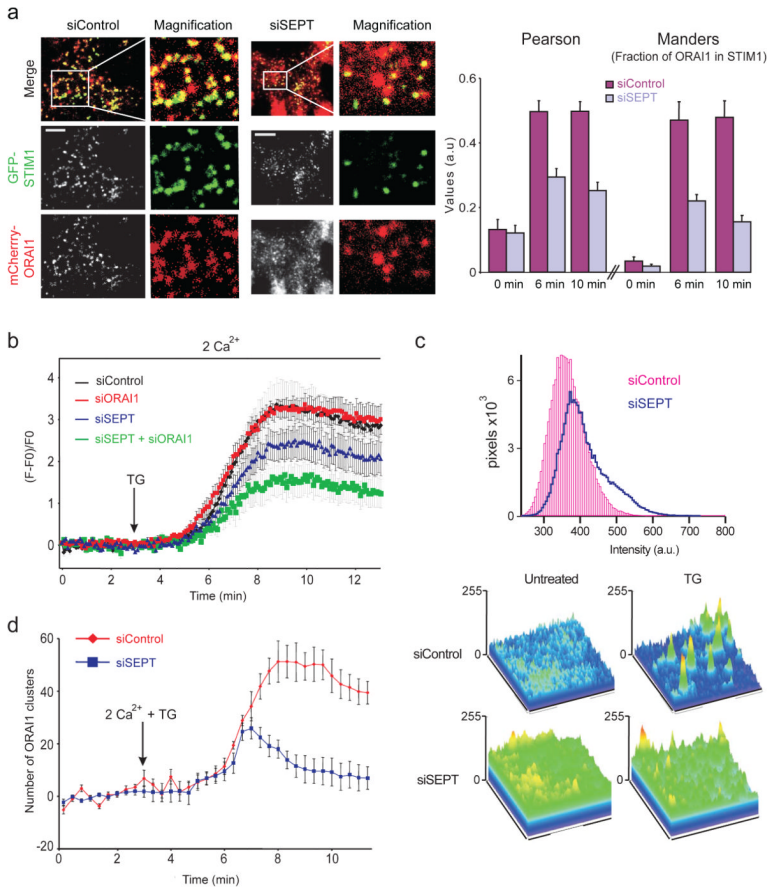

Figure 2. Septin depletion impairs STIM1-ORAI1 colocalisation at ER-plasma membrane junctions

a, (*Left*) Single-channel, merged, and magnified TIRFM images of GFP-STIM1 and mCherry-ORAI1 distribution in siRNA-treated HeLa cells stimulated for 10 min with TG. (*Right*) Statistical analyses of STIM1 and ORAI1 colocalisation using Pearson's coefficient (*siSEPT vs siControl*: 0 min, $p=0.77$; 6 min, $p=1.8\times10^{-4}$; 10 min, $p=7.4\times10^{-6}$) and Manders coefficient (*siSEPT vs siControl*: 0 min, $p=0.3$; 6 min, $p=4.7\times10^{-3}$; 10 min, $p=1.5\times10^{-4}$). **b**, Averaged kinetics of GFP-STIM1 fluorescence at the TIRF layer in siRNA-treated Hela cells (*siControl*, *n=25; siSEPT*, *n=18; siORAI1*, *n=35; siSEPT/ORAI1*, *n=28*). **c**, Histogram and surface plots of mCherry-ORAI1 pixel intensities from TIRFM images of siRNA-treated HeLa cells expressing GFP-STIM1 and mCherry-ORAI1. **d**, Quantification of mCherry-ORAI1 cluster formation at the TIRF layer in HeLa cells expressing GFP-STIM1 and mCherry-ORAI1. Error bars report s.d. (**a**) or standard error of the mean (s.e.m.) (**b**,**d**).

NIH-PA Author Manuscript

NIH-PA Author Manuscript

NIH-PA Author Manuscript

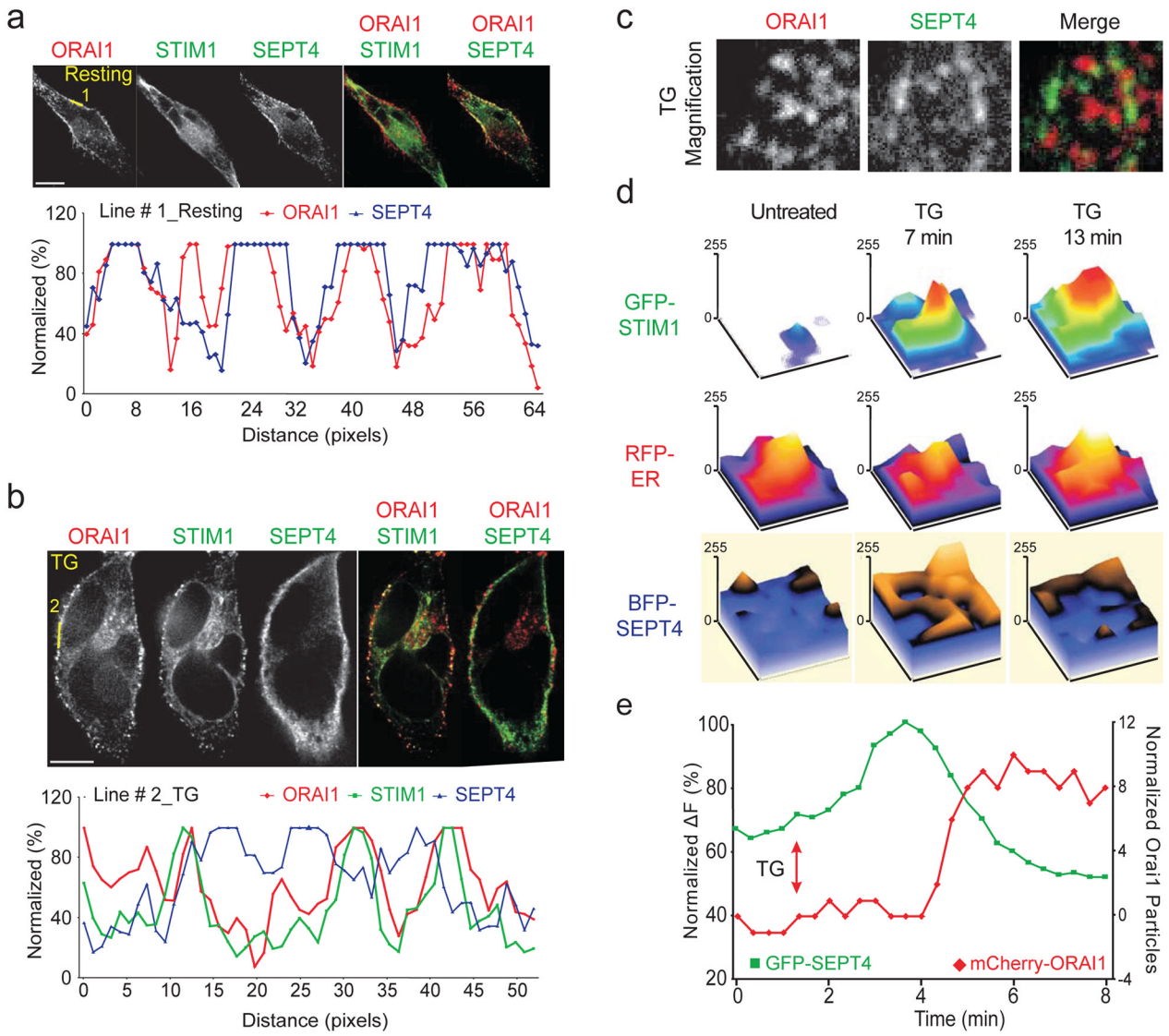

Figure 3. Septin 4 relocalises at the plasma membrane after ER Ca^{2+} store depletion

a and **b**, (*Upper*) Single-channel and merged confocal images of HeLa cells expressing mCherry-ORAI1, GFP-STIM1 and FLAG-SEPT4, unstimulated (**a**) or stimulated for 10 min with TG (**b**). (*Lower*) Normalised pixel intensities along the indicated line scans. **c**, Single-channel and merged TIRFM images of HeLa cells expressing mCherry-ORAI1, STIM1 (not shown) and GFP-SEPT4 after 10 min of TG stimulation. **d**, Surface plots of pixel intensities from TIRFM images of HeLa cells expressing GFP-STIM1, RFP-ER and BFP-SEPT4, before and after stimulation with TG in 0 mM $[Ca^{2+}]_o$. **e**, Kinetics of GFP-SEPT4 fluorescence (*green trace*) and mCherry-ORAI1 particle number (*red trace*) at the TIRF layer in a typical cell. A time series of images of this cell is shown in Supplementary Figure 6b.

NIH-PA Author Manuscript

NIH-PA Author Manuscript

NIH-PA Author Manuscript

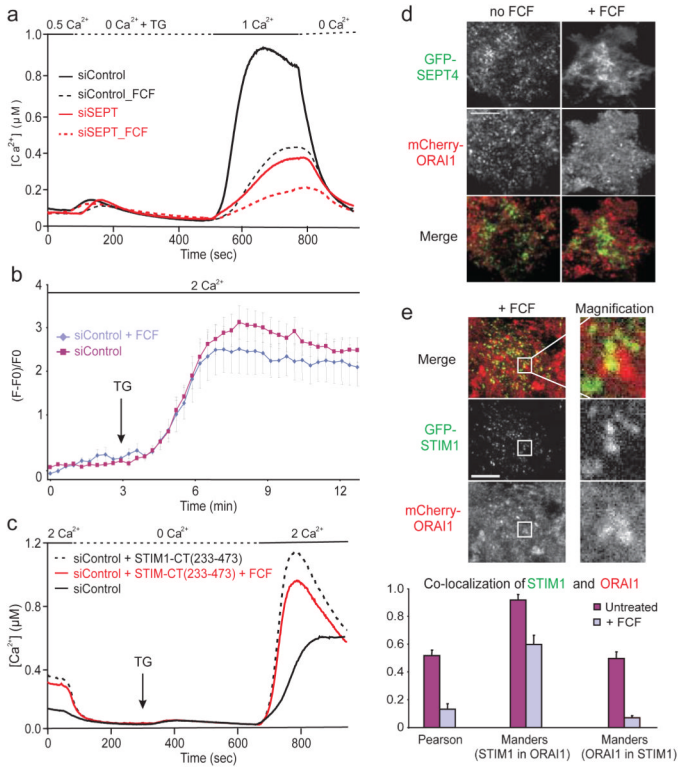

Figure 4. Rearrangement of septin 4 at the plasma membrane is required for ORAI1 cluster formation

a, Single-cell $[Ca^{2+}]_i$ measurements in untreated or forchlorfenuron (FCF)-pretreated, fura-2 loaded HeLa cells (*n>75*). **b**, Averaged kinetics of GFP-STIM1 fluorescence at the TIRF layer in untreated or FCF-pretreated HeLa cells expressing mCherry-ORAI1 and GFP-STIM1 (*siControl*, *n=8; siControl + FCF*, *n=12*). Error bars report s.e.m. **c**, Single-cell $[Ca^{2+}]_i$ measurements in fura-2 loaded HeLa cells transfected with mCherry-STIM1-CT(233–473) plasmid, and left untreated or pretreated with FCF (*n>75*). **d**, Single-channel and merged TIRFM images of GFP-SEPT4 and mCherry-ORAI1 in HeLa cells left untreated or pretreated with FCF, then stimulated with TG for 6 min. A time series, with images of the same cells prior to stimulation and at 2 min and 6 min TG stimulation, is displayed in Supplementary Figure 7. **e**, (*Upper*) Single-channel and merged TIRFM images of GFP-STIM1 and mCherry-ORAI1 distribution in FCF-treated HeLa cells, after stimulation with TG for 10 min; *right panels*, magnifiied view of the boxed region. (*Lower*) Statistical analyses of STIM1 and ORAI1 colocalisation in FCF-treated *vs* untreated cells (Pearson, $p=3.0\times10^{-23}$; Manders (STIM1 in ORAI1), $p=6.3\times10^{-5}$; Manders (ORAI1 in STIM1), $p=1.4\times10^{-10}$). Error bars report s.d.

NIH-PA Author Manuscript
NIH-PA Author Manuscript
NIH-PA Author Manuscript

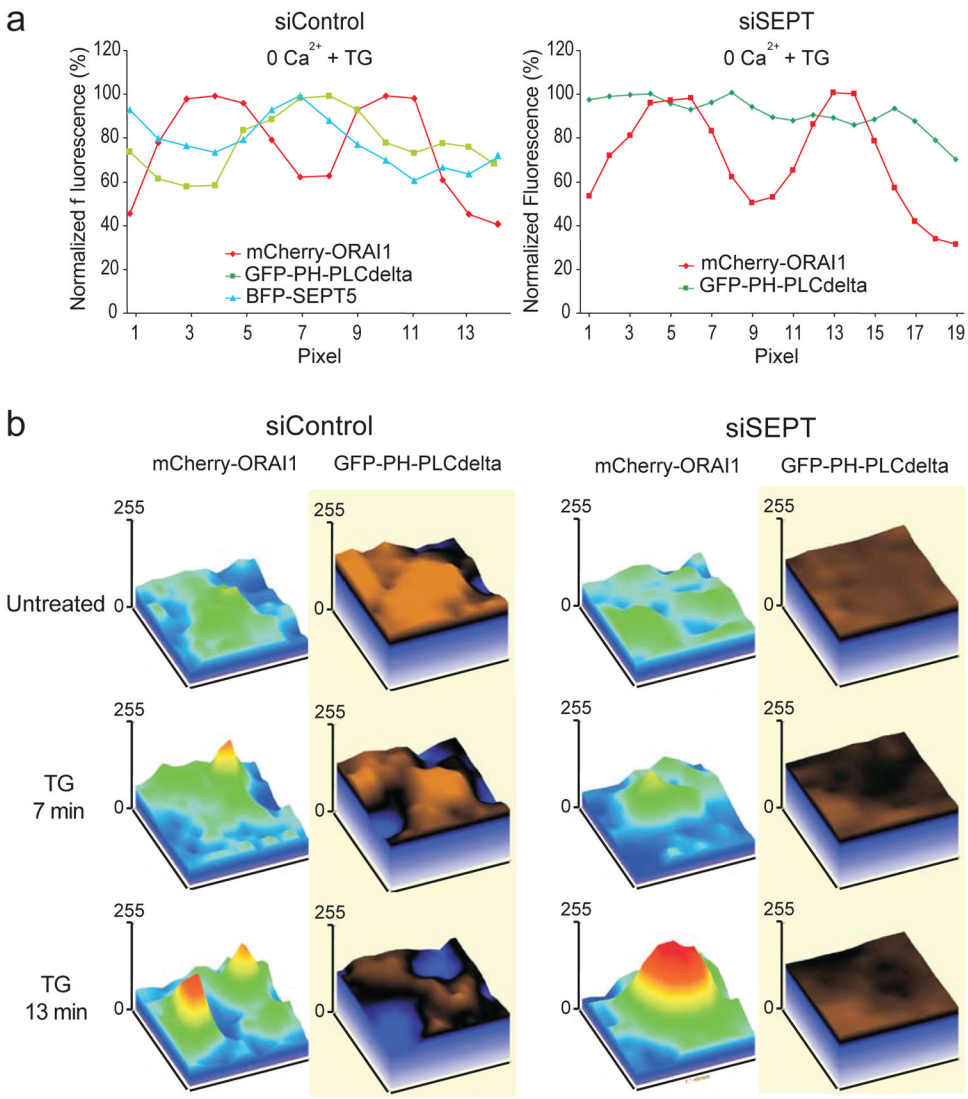

Figure 5. Septins organise PIP2 domains surrounding STIM1-ORAI1 clusters at ER-plasma membrane junctions

a, Normalised pixel intensities from TIRFM images of HeLa cells transfected with *siControl*, mCherry-ORAI1, BFP-SEPT5 and GFP-PH-PLCδ (*left*) or *siSEPT*, mCherry-ORAI1 and GFP-PH-PLCδ (*right*), and stimulated with TG in 0 mM Ca^{2+}. **b**, Surface plots of mCherry-ORAI1 and GFP-PH-PLCδ pixel intensities from TIRFM images of siRNA-treated HeLa cells, before and after stimulation with TG in 0 mM Ca^{2+}.